

Liquid nucleation around charged particles in the vapor phase

Roni Kroll¹ and Yoav Tsori¹

Department of Chemical Engineering, Ben-Gurion University of the Negev, Beersheba,
Israel.

Dated: 4 November 2021

We theoretically investigate the nucleation of liquid droplets from vapor in the presence of a charged spherical particle. Due to field gradients, sufficiently close to the critical point of the vapor–gas system, the charge destabilizes the vapor phase and initiates a phase transition. The fluid’s free energy is described by the van der Waals expression augmented by electrostatic energy and a square-gradient term. We calculate the equilibrium density profile at arbitrary temperatures, particle charges, and vapor densities. In contrast to classical nucleation theory, here, both liquid and vapor phases are different from the bulk phases because they are spatially nonuniform. In addition, the theory applies to both sharp and diffuse interfaces and calculates the surface tension self-consistently. We find the composition profiles and integrate them to get the adsorption near the particle. We find that the adsorption changes discontinuously at a first-order phase transition line. This line becomes a second-order phase transition at high enough temperatures. We describe the transition point numerically and provide approximate analytical expressions for it. Similarly to prewetting, the adsorption diverges at the binodal phase boundary. We construct a phase diagram indicating changes in the binodal, spinodal, and critical temperature. It is shown that the field gradient enlarges the range of temperature and vapor density where liquid can nucleate.

I. INTRODUCTION

Nucleation is a thermodynamic process that constitutes the initial step for many physical processes, such as vapor condensation, melting, and boiling.^{1–4} It is a localized phase transition process that occurs at metastable conditions, where the system has an energy barrier to overcome to reach its equilibrium state. Heterogeneous nucleation occurs in the presence of foreign objects, such as the walls of a vessel, dust particles, or other impurities. The presence of foreign particles reduces the nucleation energy barrier locally and, consequently, the supersaturation required for the nucleation. The rate of the critical nuclei creation is proportional to the exponential of the ratio between the barrier and thermal energies. Heterogeneous nucleation can be relatively fast, and in many cases, it is the dominant mechanism.^{5,6}

A commonly used model for nucleation is the classical nucleation theory (CNT) based on the work of Volmer and Weber, Becker and Döring and Frenkel.^{7–9} The CNT model describes the condensation of vapor to liquid nucleus. The nucleus, assumed to be spherical, is described by the macroscopic properties of the stable phase. The interface between the liquid and vapor phases is considered to be spherical with zero thickness, independent of the nucleus size.

The Thomson model is an extension of CNT theory that includes the charge of the nucleating particle. In the Thomson model, the Gibbs transfer energy for the transfer of molecules from vapor to liquid around the charged particle is given by¹⁰

$$\Delta G = -\frac{4\pi R_i^3}{3v} k_B T \ln(P/P^*) + 4\pi R_i^2 \gamma + \frac{q^2}{8\pi\epsilon_0} \left(\frac{1}{\epsilon_1} - \frac{1}{\epsilon_2} \right) \left(\frac{1}{R_i} - \frac{1}{R} \right). \quad (1)$$

The first term represents a bulk free energy: $4\pi R_i^3/3v$ is the number of molecules in a liquid nucleus with radius R_i , where

v is the volume of a single molecule, and P/P^* is the vapor supersaturation ratio. The second term is a surface energy, where γ is the surface tension between liquid and vapor. The third term is the electrostatic energy of a spherical particle of radius R and charge q purely embedded in a dielectric fluid. ϵ_1 and ϵ_2 are the relative dielectric constants of pure gas and liquid, respectively, and ϵ_0 is the permittivity of the vacuum.

The nucleation process, in the absence of external forces, happens in supersaturated systems ($P/P^* > 1$). Once the conditions for nucleation exist, the Thomson model predicts the infinite growth of the radius as the Gibbs transfer energy is decreasing as a function of R_i . Figure 1(a) shows the three energy contributions of the Thomson model in the metastable region of the phase diagram and their sum including the electrostatic term (black curve). A local minimum occurs at a finite radius R_i , but the most stable nucleus size is infinite. Figure 1(b) shows the same energy contributions when the bulk conditions are not metastable, that is, in the stable vapor phase. In this case, the bulk term, $\sim R_i^3$, is positive, and due to the electrostatic term, the global minimum occurs at a finite nucleus radius R_i . The size of this nucleus vs $\sigma^2/2P_c\epsilon_0$ is displayed in Fig. 1(c), where σ is the surface charge density of the charged particle.

Experimental work in different fields such as polymer crystallization and atmospheric science confirmed that electrostatic interactions promote nucleation.^{11,12} This article generalizes the Thomson nucleation model. Near charged particles, field gradients lead to coupling between the electric field and the density of the fluid. The dielectric fluid is attracted by a dielectrophoretic force to the charged surface, leading to an increase in the density. In return, the density affects the electric field through the change in the dielectric constant.¹³ Below, we demonstrate how this phenomenon provokes the phase transition and enlarges the range of temperatures and densities where vapor and liquid coexist. We use the van der Waals mean-field energy supplemented by square-gradient

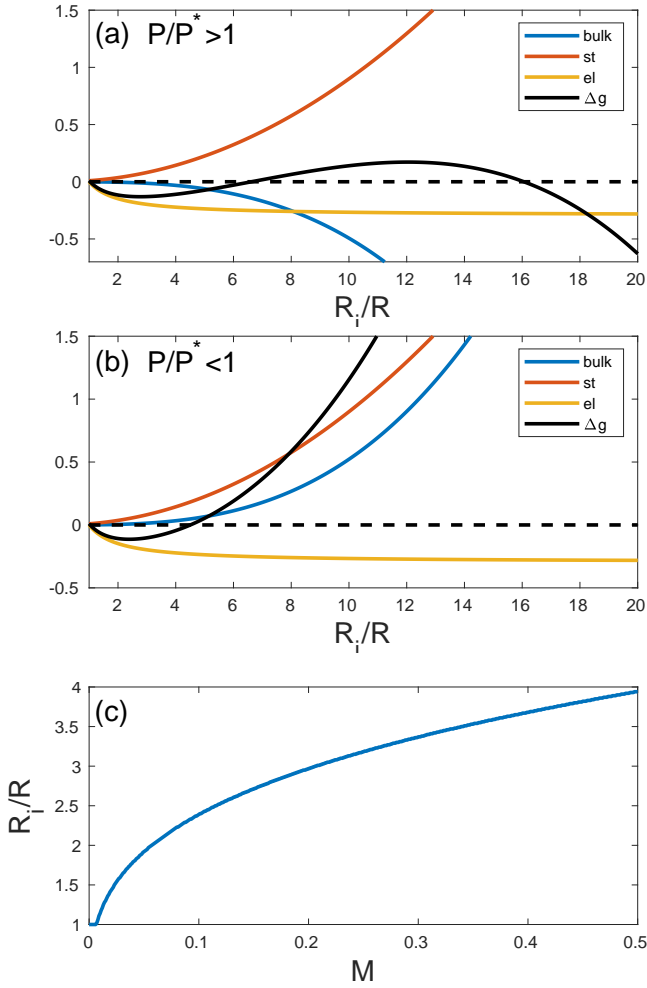


FIG. 1. Different contributions to the energy in the Thomson model Eq. (1). (a) For a supersaturated system, $\phi_0 = 0.856$ and $M = 0.1$. Legend labels “bulk”, “st”, “el”, and “ Δg ” represent the mixing, surface tension, electrostatic, and total Gibbs energies, respectively. (b) The same as in (a) but for an unsaturated system $\phi_0 = 0.850$. (c) The nucleus radius as a function of $M \equiv \sigma^2/2P_c\epsilon_0$, where σ is the surface charge density of the charged particle. We used $\phi^* = 0.853$, $T/T_c = 0.995$, and $\gamma/(RP_c) = 3 \times 10^{-3}$.

theory. We extremize the free energy and solve the Euler–Lagrange equations to obtain the thermodynamically stable solutions.

II. MODEL

We investigate the liquid–vapor pure component system by using the classical van der Waals mean-field model. The fluid is characterized by its temperature T and its number density ρ . The fluid surrounds a perfect solid sphere with radius R that is uniformly charged with surface charge density σ . The Helmholtz free energy of a one component van der Waals fluid around a charged particle is the integral over space of the sum

energy densities. Smooth density profiles, not considered by the CNT model, are allowed here by inclusion of a square-gradient term,¹⁴

$$F = \int \left[\frac{1}{2}c^2|\nabla\rho|^2 + f_{\text{vdw}} + f_{\text{es}} \right] dr. \quad (2)$$

Here, c is a constant and f_{vdw} is the van der Waals free energy density given by¹⁵

$$f_{\text{vdw}} = k_B T \rho \left[\log(\rho\Lambda^3) - 1 - \log(1 - \rho b) \right] - a\rho^2. \quad (3)$$

Here, k_B is the Boltzmann constant, T is the temperature, and Λ is the thermal de Broglie wavelength. The parameters a and b are positive constants where a accounts for the attractive forces between the molecules and b represents the excluded volume of the molecules. a and b are related to the critical temperature T_c and density ρ_c by $(T_c, \rho_c) = (8a/(27k_B b), (3b)^{-1})$. From the van der Waals equation of state $(P + a\rho^2)(1 - b\rho) = \rho k_B T$, the value of the critical pressure is found to be $P_c = a/(27b^2)$.

The electrostatic energy density of a perfect dielectric fluid is

$$f_{\text{es}} = \frac{1}{2}\epsilon_0\epsilon\mathbf{E}^2, \quad (4)$$

where $\mathbf{E} = -\nabla\psi$ is the electric field, ψ is the electrostatic potential, and $\epsilon(\rho)$ is the relative dielectric constant. The system is open and has a vapor phase with constant density far from the particle surface. The thermodynamically stable solutions are minimizers of the grand canonical energy $\Omega = F - \mu N$, where μ is the chemical potential and N is the number of fluid molecules. Extremization of Ω with respect to density and electrostatic potential yields two coupled Euler–Lagrange equations,

$$\frac{\delta\Omega}{\delta\rho} = -c^2\nabla^2\rho + \frac{\partial f_{\text{vdw}}}{\partial\rho} - \frac{1}{2}\epsilon_0\frac{d\epsilon}{d\rho}|\nabla\psi|^2 - \mu = 0, \quad (5)$$

$$\frac{\delta\Omega}{\delta\psi} = \nabla \cdot (\epsilon_0\epsilon(\rho)\nabla\psi) = 0. \quad (6)$$

Equation (6) represents the Laplace equation. The spherical symmetry allows us to describe the system in one dimension, with variations only in the r coordinate; hence, the solution for the electric field, given by $\mathbf{E} = \sigma R^2/r^2\epsilon_0\epsilon(\rho)\hat{\mathbf{r}}$, is decaying as $\sim r^{-2}$. We use $\phi \equiv \rho/\rho_c$ as the reduced density and substitute the electric field into Eq. (5) to get

$$-\tilde{c}^2\tilde{\nabla}^2\phi + \frac{\partial\tilde{f}_{\text{vdw}}}{\partial\phi} - M\frac{d\epsilon/d\phi}{\epsilon(\phi)^2}\tilde{r}^{-4} - \tilde{\mu} = 0, \quad (7)$$

where the tilde sign indicates reduced quantities: $\tilde{f}_{\text{vdw}} = f_{\text{vdw}}/P_c$, $\tilde{r} = r/R$, $\tilde{c}^2 = c^2\rho_c^2/P_cR^2$ and $\tilde{\mu} = \mu\rho_c/P_c$. In addition, we define

$$M = \sigma^2/2P_c\epsilon_0 \quad (8)$$

as the dimensionless electrostatic energy. The boundary conditions for the equation are as follows:

$$\begin{aligned} \tilde{r} = 1, & \quad -\hat{n} \cdot (-\tilde{c}^2\nabla\phi) = 0, \\ \tilde{r} = \infty, & \quad \phi = \phi_0, \end{aligned} \quad (9)$$

where \hat{n} is a unit vector perpendicular to the surface of the particle. The first boundary condition means zero flux on the surface of the particle, while the second boundary enforces the bulk reservoir density ϕ_0 at infinity.

The local dielectric constant $\varepsilon(\phi)$ depends on the local value of the density and on the dielectric constants of the pure phases, ε_1 (gas) and ε_2 (liquid). We assume a linear relation between the local dielectric constant and the fluid density, $\varepsilon = \varepsilon_1 + \Delta\varepsilon\phi/3$, where $\Delta\varepsilon = \varepsilon_2 - \varepsilon_1$ is a constant (recall that $0 \leq \phi \leq 3$). In thermodynamic equilibrium, the chemical potential is constant everywhere. In the grand canonical ensemble, it is found from $\tilde{\mu} = \partial \tilde{f}_{\text{vdw}}(\phi_0)/\partial \phi$ with $\tilde{r} \rightarrow \infty$ where the electric field tends to zero and the density tends to the vapor reservoir density ϕ_0 .

III. RESULTS AND DISCUSSION

A. Linearization of ϕ

We focus on a charged particle in the presence of a stable vapor phase. For small enough particle potentials, the fluid's density will not change sharply in space, and in this case one can linearize the Euler–Lagrange equations around the bulk value of ϕ . Substitution of $\phi = \phi_0 + \delta\phi$, with $\delta\phi \ll \phi_0$, into Eq. (7) leads to a linear differential equation for $\delta\phi$,

$$\tilde{\nabla}^2 \delta\phi - A\delta\phi + B\tilde{r}^{-4} = 0, \quad (10)$$

where A and B are given by $A = \left(\frac{24T/T_c}{\phi_0(3-\phi_0)^2} - 6\right)/\tilde{c}^2$ and $B = M\Delta\varepsilon/(3\varepsilon^2\tilde{c}^2)$. The general solution for Eq. (10) is given by

$$\delta\phi = C \frac{e^{-\sqrt{A}\tilde{r}}}{\tilde{r}} + \frac{\sqrt{AB}}{4\tilde{r}} \left[-e^{\sqrt{A}\tilde{r}} Ei(-\sqrt{A}\tilde{r}) + e^{-\sqrt{A}\tilde{r}} Ei(\sqrt{A}\tilde{r}) \right] - \frac{B}{2\tilde{r}^2}, \quad (11)$$

where the first term represents the homogeneous solutions and the rest represents the particular solution. Ei is the exponential integral defined as $Ei(x) = \int_{-\infty}^x (e^t/t) dt$. The constant C is found from the boundary condition $\partial \delta\phi / \partial \tilde{r}|_{\tilde{r}=1} = 0$,

$$C = -\frac{1}{4}\sqrt{AB} \left[\frac{\sqrt{A}-1}{\sqrt{A}+1} e^{2\sqrt{A}} Ei(-\sqrt{A}) + Ei(\sqrt{A}) \right] + B \frac{e^{\sqrt{A}}}{\sqrt{A}+1}. \quad (12)$$

B. Nonlinear profiles in the sharp interface limit

The linear profiles in Eq. (12) are valid when the density changes are small, but when the electro-prewetting transition occurs and liquid wets the particle, this assumption falls, and one needs to solve Eq. (7) numerically. The density profiles are calculated by setting the values of ϕ_0 , M , and T/T_c and, then, finding the solutions $\phi(\tilde{r})$ for all \tilde{r} . When $\tilde{c} = 0$, for small or large values of \tilde{r} , there is only one solution. However, if M

is large enough for intermediate values of \tilde{r} , there is more than one solution to the equation. At these \tilde{r} 's, we calculated the energy for each of the solutions and selected the equilibrium solution as the one with minimal energy.

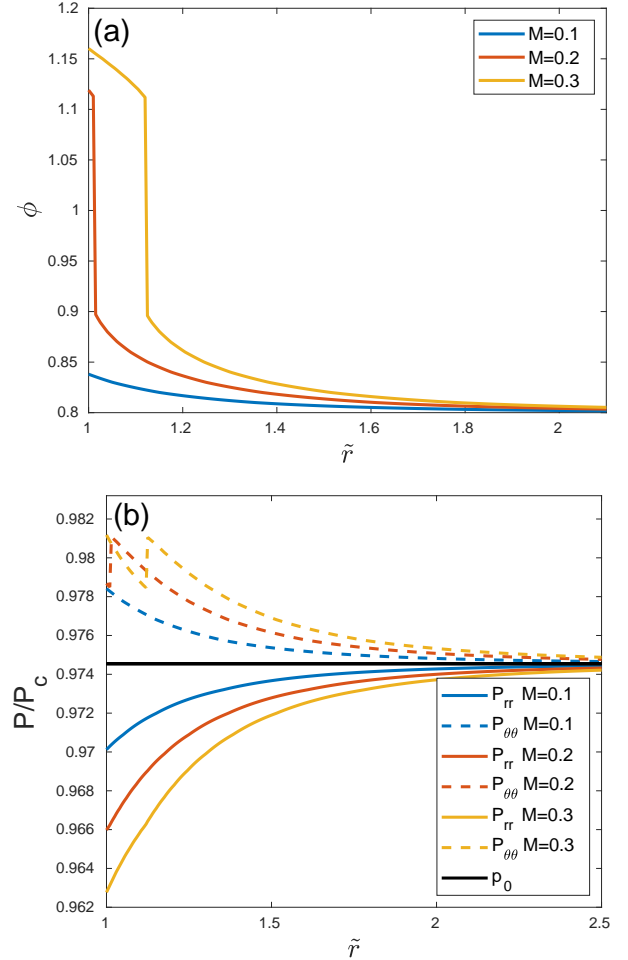


FIG. 2. (a) Equilibrium density profiles $\phi(\tilde{r})$ in the sharp interface limit, $\tilde{c} = 0$, at a temperature of $T/T_c = 0.995$ and bulk density of $\phi_0 = 0.8$. (b) Radial p_{rr} and azimuthal $p_{\theta\theta}$ pressure profiles corresponding to the density profiles in (a). $\varepsilon_1 = 1$ and $\varepsilon_2 = 80$ in this and in all other figures.

Fig. 2(a) shows the numerically obtained density profiles in the sharp interface limit, $\tilde{c} = 0$. At small values of M (small particle charge), the density is smoothly varying at all values of \tilde{r} . At large enough values of M , a dense phase appears on the surface of the particle in coexistence with a vapor phase far from it. Note that both phases are spatially nonuniform and cannot be described by the bulk phases, liquid or vapor. The interface between the two phases exhibits a sharp jump in the density. We denote by R_i the location of the vapor–liquid interface. Due to the dielectrophoretic force, an increase in M “draws” more molecules to the region with strong electric field, resulting in a larger nucleus.

In Fig. 2(b), we show the pressure profiles. When a fluid is under an electric field, stress develops. The stress tensor is

given by¹⁶

$$T_{ij} = -p_0(\phi, T)\delta_{ij} + \frac{1}{2}\epsilon E^2 \left(-1 + \frac{\phi}{\epsilon} \left(\frac{\partial \epsilon}{\partial \phi} \right) \right) \delta_{ij} + \epsilon E_i E_j, \quad (13)$$

where p_0 is the bulk (zero charge) pressure given by $p_0 = \phi_0 \partial f_{\text{vdw}}(\phi_0) / \partial \phi - f_{\text{vdw}}(\phi_0)$. δ_{ij} is the Kronecker delta function. The diagonal pressure components in the rr and $\theta\theta$ axis are

$$p = p_0(\phi, T) - M \left[\pm \frac{1}{\epsilon} + \frac{\phi}{\epsilon^2} \left(\frac{\partial \epsilon}{\partial \phi} \right) \right] \tilde{r}^{-4}, \quad (14)$$

where the (+) sign is for p_{rr} and (−) sign for $p_{\theta\theta}$. The pressure profiles are discontinuous when a sharp interface is created. The discontinuity in p_{rr} is small.

Figure 3(a) shows the finite radius R_i of the nucleus as a function of M , obtained from the solutions of Eq. (7) in the sharp interface limit. As the value of ϕ_0 decreases, that is, P/P^* decreases, a larger value of M is needed for nucleation to occur. For the same M , a larger radius is obtained as the saturation ratio grows. In Fig. 3(b), we keep M constant and vary the temperature. The radius of the drop R_i increases when T decreases. For each value of ϕ_0 , the lowest temperature shown is the binodal temperature, below which phase coexistence occurs even without the driving force of the electric charge. Below the binodal, the equilibrium nucleus size becomes infinite.

C. Diffuse interface profiles

Experimental data show that the nucleation rate in some cases deviate by several orders of magnitude from the CNT theory.^{17,18} The source of the deviation is presumably the “capillarity” approximation, i.e., the assumption that the bulk surface tension of the nucleus equals the surface tension of a thin and flat interface. One popular approach to avoid these assumptions is to use the density functional theory (DFT), but it requires knowledge of intermolecular potentials.^{19,20} Another approach, is the phenomenological diffuse interface theory, which has proven as reliable over many length-scales.²¹ We now release the assumption $\tilde{c} = 0$ and solve the full equation Eq. [(7)] including the square-gradient term. This term is connected to changes in the density and adds the interfacial contribution to the free energy. In spherical symmetry, the nonlinear static equation is solved in one dimension using finite elements and Newton–Raphson iterations. For numerical purposes, the maximum value of \tilde{r} was taken as $\tilde{r} = 10$, and indeed the gradient $|\phi'|$ was verified as negligibly small in these “large” distances.

The density profiles for the case where $\tilde{c}^2 = 10^{-3}$ are presented in Figs. 4(a) and 4(b). In contrast to the CNT model, here, the density of both liquid and vapor phases is spatially varying, and the interface between them is smooth. We computed profiles for different values of bulk composition ϕ_0 in iterations. The initial guess for the profile of each value of ϕ_0 is taken as the solution of the previous iteration. Figures 4(a) and 4(b) show the same values of M , T/T_c , and ϕ_0 , but

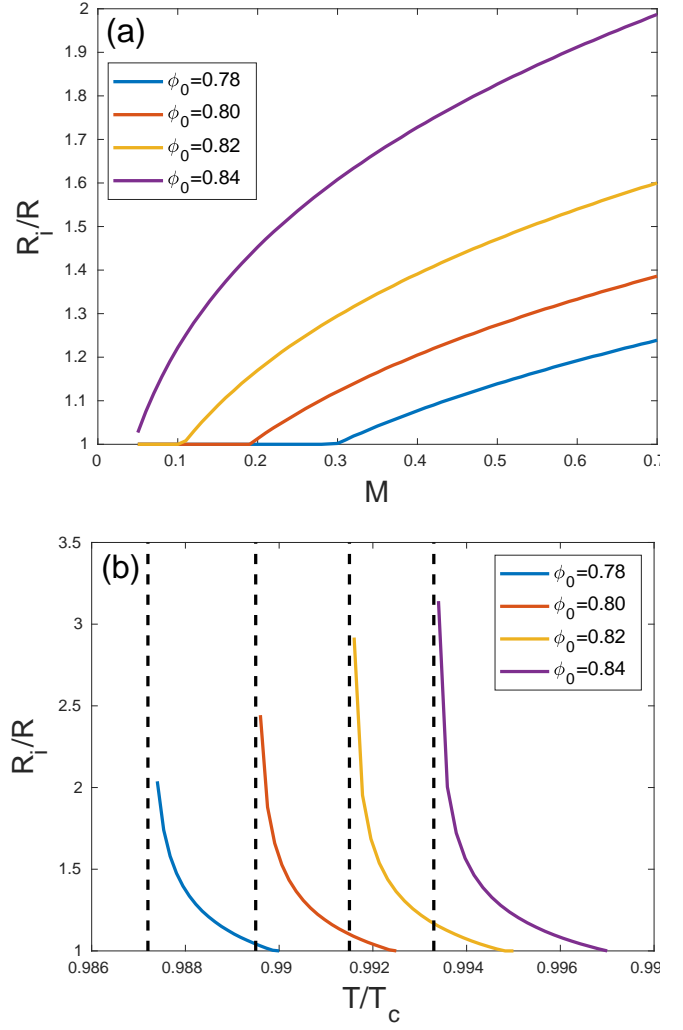


FIG. 3. (a) Location of the interface R_i in the sharp interface limit, $\tilde{c} = 0$, as a function of the scaled particle charge M at fixed temperature given by $T/T_c = 0.995$ for several values of the average composition ϕ_0 . (b) Similar to (a) but now R_i as a function of T/T_c at fixed $M = 0.1$.

in Fig. 4(a), ϕ_0 was increased in the iterations from unsaturated conditions to supersaturation, while in Fig. 4(b), ϕ_0 was reduced. This procedure leads to differences in the profiles in the range $\phi_0 = 0.865 - 0.867$. In this range, the system is in a metastable state in Fig. 4(a). The energies of the profiles in Fig. 4(b) are lower, indicating that these are the equilibrium solutions for these conditions.

Once profiles are found, one can calculate the adsorption Γ , given by the following expression:

$$\Gamma = 4\pi \int_1^\infty (\phi(\tilde{r}) - \phi_0) \tilde{r}^2 d\tilde{r}. \quad (15)$$

The adsorption is shown in Fig. 5 as a function of bulk composition ϕ_0 and for several temperatures (see the legend of Fig. 5). At temperatures sufficiently lower than T_c , $\Gamma(\phi_0)$ increases slowly with ϕ_0 until a certain critical composition is reached. At this composition, Γ rises up sharply, which is the signature

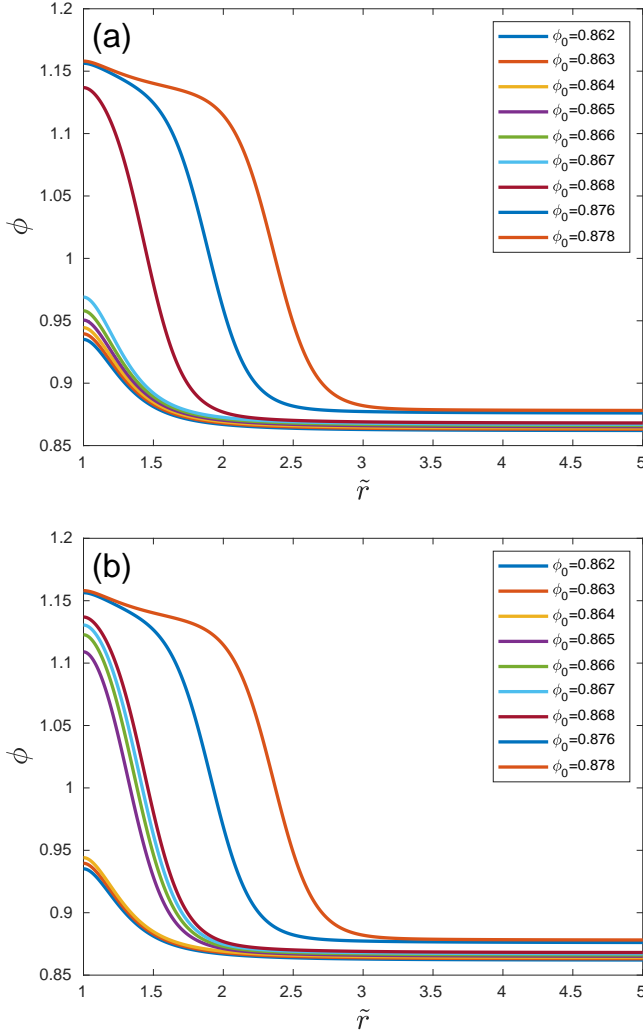


FIG. 4. Density profiles for a diffuse interface when $T/T_c = 0.996$, $M = 0.1$, and $\tilde{c}^2 = 0.001$. The initial guess for the iterations is taken as the solution of the previous iteration where ϕ_0 is increasing (a) or decreasing (b).

of the first-order phase transition (due to the deficiency of numerical schemes, the discontinuous jump has a finite width). Above the transition, Γ continues to increase until, when ϕ_0 equals the binodal composition at that particular temperature (the right-most point in every curve), it diverges. This behavior is reminiscent of the classical prewetting transition near a surface with short-range interactions.^{22–24} At temperatures sufficiently close to T_c , however, the transition is a continuous second-order transition, as should be expected in the presence of long-range forces.

D. Phase diagram

In the absence of a charged particle, the phase equilibrium is given by the following classical common-tangent construc-

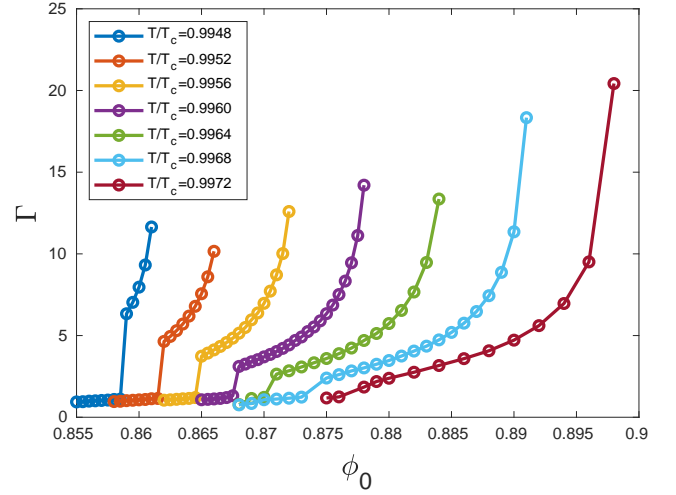


FIG. 5. Adsorption Γ from Eq. (15) vs bulk composition at different temperatures (see the legend). For a particular temperature, Γ increases with ϕ_0 for sufficiently small values of ϕ_0 . At the first-order transition line, it “jumps” discontinuously to higher values. Above this threshold composition, Γ continuously increases with ϕ_0 . It diverges at the binodal composition. For sufficiently high temperatures, given by Eq. (17), the first-order line becomes second-order, and the transition becomes smooth ($T/T_c = 0.9972$). We used $M = 0.1$ and $\tilde{c}^2 = 0.001$.

tion:

$$\begin{aligned} \frac{\partial f_{\text{vdw}}(\phi_1)}{\partial \phi} - \mu &= 0, \\ \frac{\partial f_{\text{vdw}}(\phi_2)}{\partial \phi} - \mu &= 0, \\ \frac{f_{\text{vdw}}(\phi_2) - f_{\text{vdw}}(\phi_1)}{\phi_2 - \phi_1} - \mu &= 0. \end{aligned} \quad (16)$$

Here, ϕ_1 and ϕ_2 are the two coexisting binodal densities for the given temperature. The spinodal curve, defined by $\partial^2 f_{\text{vdw}} / \partial \phi^2 = 0$, is below the binodal. While under the spinodal, phase separation is spontaneous, the area between the spinodal and binodal curves is metastable and liquid appears by nucleation.

The presence of a charged particle induces phase separation, and this modifies the phase diagram. Figure 6(a) shows the new phase diagram in the sharp interface limit. In the presence of a charged particle, we call the coexistence curve the “stability curve.” The stability curves for different values of M appear as colored lines. Point (ϕ_0, T) above the stability curve is stable (the particle is surrounded by a vapor phase), while below this curve, the point is unstable and nucleation occurs (the particle is wetted by a dense phase). An increase in M enlarges the range of conditions where nucleation occurs. While under the binodal, the radius of nucleation is infinite, in the area between the binodal and the stability curve, droplets with finite radius nucleate. The black solid line in Fig. 6 represents the “electrostatic binodal.” This curve represents the stability line for the limit $M \rightarrow \infty$. This means that for a point (ϕ_0, T) above the electrostatic binodal, there is no value of M that can

lead to nucleation.²⁵

The critical point is modified in the presence of charge. The “kink point” is the point where the first-order transition line becomes a second-order transition. In the sharp interface limit, this point is defined by the pair of values $(\phi_0, T/T_c)$ that sets to zero the value of the second and third derivatives of \tilde{f} at $\tilde{r} = 1$,

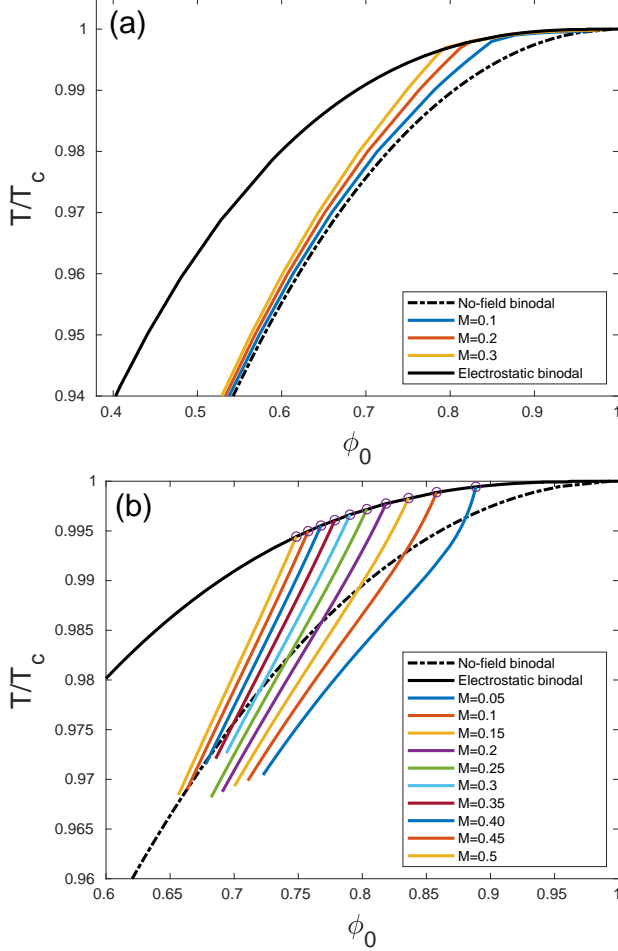


FIG. 6. (a) Stability diagram in the sharp interface limit. The black dashed-dotted line represents the classical no-field binodal curve. The black solid line is the electrostatic binodal. The colored lines represent the stability curves for different values of M . Under the stability curves, liquid–vapor coexistence is thermodynamically preferred. (b) Electrostatic spinodals in the sharp interface limit for different values of M . Under the electrostatic spinodal, the system spontaneously separates to two phases, while above it, it is in a metastable state.

$$\begin{aligned} \frac{\partial \tilde{f}_{\text{vdw}}(\phi_s)}{\partial \phi} - \frac{M\Delta\epsilon}{3\epsilon(\phi_s)^2} - \frac{\partial \tilde{f}_{\text{vdw}}(\phi_0)}{\partial \phi} &= 0, \\ \frac{\partial^2 \tilde{f}_{\text{vdw}}(\phi_s)}{\partial \phi^2} + \frac{2M\Delta\epsilon^2}{9\epsilon(\phi_s)^3} &= 0, \\ \frac{\partial^3 \tilde{f}_{\text{vdw}}(\phi_s)}{\partial \phi^3} - \frac{2M\Delta\epsilon^3}{9\epsilon(\phi_s)^4} &= 0, \end{aligned} \quad (17)$$

where $\phi_s = \phi(\tilde{r} = 1)$ is the surface composition.

In the reduced quantities used by us, the value of the bulk critical point without a charge is $(\phi_c, T/T_c) = (1, 1)$. When M is sufficiently small, the value of the kink point on the colloid surface can be found analytically by substituting $T/T_c = 1 + \Delta t$ and $\phi = 1 + \Delta\phi$ in Eq. (17) to get

$$\begin{aligned} \Delta t &\approx -\frac{M\Delta\epsilon^2}{27\epsilon_c^3}, \\ \Delta\phi &\approx \frac{2M\Delta\epsilon^3}{81\epsilon_c^4}, \end{aligned} \quad (18)$$

where $\epsilon_c = \epsilon(\phi = 1) = \epsilon_1 + \Delta\epsilon/3$. The kink points for different values of M are shown as circles in Fig. 6(b).

The kink point is the end of another curve, the “electrostatic spinodal.” The electrostatic spinodal, in a manner similar to the regular non-field case, divides the two-phase region to the area where the spontaneous and non-spontaneous nucleation occurs, as shown in Sec. III C. When $\tilde{c} = 0$ and for a fixed temperature, it can be calculated analytically looking for the value of ϕ_0 that leads to $\partial^2 f(\tilde{r} = 0)/\partial \phi^2 = 0$ at the surface of the colloid ($\tilde{r} = 1$). For non-zero \tilde{c} , we find it by looking at the parameters that cause phase separation when the initial guess is the uniform vapor density ϕ_0 .

Figure 7 shows the phase diagrams in both the sharp interface and diffuse interface limits. While the electric charge enlarges the area where phase separation is favorable, the existence of the $(\nabla\phi)^2$ term leads to an effective surface tension and to reduction in this area. Note that the change to the two-phase boundaries due to electric charge is appreciable relatively close to T_c , while the change in the electrostatic spinodal is significant at all temperatures. This can have an impact on supersaturated processes far from the critical temperature such as aerosol creation in clouds.²⁶

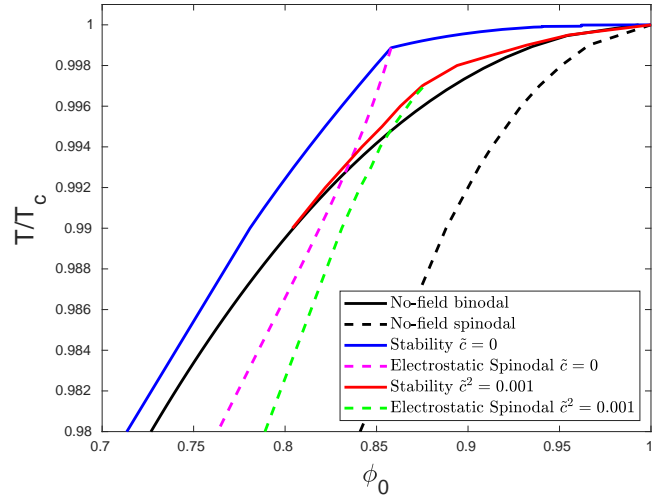


FIG. 7. Comparison between the stability curves for the sharp interface limit (blue) and the diffuse interface (red) with $M = 0.1$. The corresponding electrostatic spinodals are in pink (sharp interface limit) and green (diffuse interface).

IV. CONCLUSIONS

We study the vapor–liquid nucleation around a charged spherical particle using a simple mean-field approach. Electric field gradients lead to spatial nonuniformities in both the liquid and vapor phases, and this significantly alters the nucleation conditions. We find a first-order phase transition line outside of the binodal curve, similar to a prewetting line. Due to the long-range nature of electrostatic forces, this line becomes a second-order line at a special “kink” point, whose location is given approximately by Eq. (17). The square-gradient approach yields diffuse-interface profiles that are more realistic than the CNT profiles and facilitates the calculation of the surface tension. For small particle and nucleus, the width of the interface can be appreciable and deviations from the CNT theory are significant. This is especially relevant close to T_c where the wetting is continuous and energy barriers can be small. From the profiles, we construct a phase diagram, including the electrostatic binodal, spinodal, and kink point, indicating changes in the two-phase equilibrium region close to T_c . The existence of a stable liquid nucleus with a finite radius is predicted even outside of the binodal curve.

We treated purely dielectric fluids. A question arises as to the effect of ionic screening. When the Debye lengths of the liquid and vapor phases are much smaller than the particle radius R , the field is localized at an exponentially thin layer at the surface of the colloid. In this limit, on large scales, the electrostatic energy should lead to an effective surface tension between the liquid and the surface. In the opposite limit, where the Debye lengths are much larger than R , one retrieves the case of dielectric liquids with the field decaying as $\sim 1/r^2$. The interesting case is the very large intermediate regime.

Further investigation of the dynamics of the nucleation process is required. Such studies can increase the accuracy of predictions of the kinetics of nuclei creation, and this may have implications in engineering applications and in atmospheric studies.

Acknowledgement

This work was supported by the Israel Science Foundation (ISF) grant No. 274/19.

Conflict of Interest

We have no conflicts of interest to disclose.

Data Availability Statement

The data that supports the findings of this study are available within the article [and its supplementary material].

¹G. Coquerel, “Crystallization of molecular systems from solution: phase diagrams, supersaturation and other basic concepts.” *Chem. Soc. Rev.* **43** 7, 2286–300 (2014).

²G. M. E. F. Jones and K. P. Galvin, “Bubble nucleation from gas cavities — a review,” *Adv. Colloid Interface Sci.* **80**, 27–50 (1999).

- ³H. R. Pruppacher, J. D. Klett, and P. K. Wang, “Microphysics of clouds and precipitation,” *Aerosol Sci. Technol.* **28**, 381–382 (1998), <https://doi.org/10.1080/02786829808965531>.
- ⁴S. T. Martin, “Phase transitions of aqueous atmospheric particles,” *Chem. Rev.* **100**, 3403–3454 (2000), pMID: 11777428, <https://doi.org/10.1021/cr990034t>.
- ⁵D. Turnbull, “Kinetics of heterogeneous nucleation,” *J. Chem. Phys.* **18**, 198–203 (1950), <https://doi.org/10.1063/1.1747588>.
- ⁶N. H. Fletcher, “Size effect in heterogeneous nucleation,” *J. Chem. Phys.* **29**, 572–576 (1958), <https://doi.org/10.1063/1.1744540>.
- ⁷M. Volmer and A. Weber, “Nucleus formation in supersaturated systems,” *J. Phys. Chem.* **119**, 277–301 (1926).
- ⁸R. Becker and W. Döring, “Kinetische behandlung der keimbildung in übersättigten dämpfen,” *Ann. Phys.* **416**, 719–752 (1935), <https://onlinelibrary.wiley.com/doi/pdf/10.1002/andp.19354160806>.
- ⁹J. Frenkel, “A general theory of heterophase fluctuations and pretransition phenomena,” *J. Chem. Phys.* **7**, 538–547 (1939), <https://doi.org/10.1063/1.1750484>.
- ¹⁰A. Laaksonen, V. Talanquer, and D. W. Oxtoby, “Nucleation: measurements, theory, and atmospheric applications.” *Ann. Rev. Phys. Chem.* **46**, 489–524 (1995).
- ¹¹G. Tosi, S. Fermi, G. Falini, J. A. Gavira Gallardo, and J. M. García Ruiz, “Crystallization of proteins on functionalized surfaces,” *Acta Crystallographica Section D* **64**, 1054–1061 (2008).
- ¹²M. Gamero-Castaño and J. F. de la Mora, “Ion-induced nucleation: Measurement of the effect of embryo’s size and charge state on the critical supersaturation,” *J. Chem. Phys.* **117**, 3345–3353 (2002), <https://doi.org/10.1063/1.1492279>.
- ¹³Y. Tsori, F. Tournilhac, and L. Leibler, “Demixing in simple fluids induced by electric field gradients,” *Nature* **430**, 544–7 (2004).
- ¹⁴J. S. Rowlinson and B. Widom, *Molecular theory of capillary* (Clarendon Press, Oxford, 1982).
- ¹⁵J. L. Barrat and J. P. Hansen, *Basic concepts for simple and complex liquids* (Cambridge University Press, 2003).
- ¹⁶L. D. Landau, E. M. Lifshitz, and L. P. Pitaevskii, *Electrodynamics of continuous media; 2nd ed.* (Butterworth, Oxford, 1984).
- ¹⁷R. Strey, P. E. Wagner, and T. Schmeling, “Homogeneous nucleation rates for n-alcohol vapors measured in a two-piston expansion chamber,” *J. Chem. Phys.* **84**, 2325–2335 (1986), <https://doi.org/10.1063/1.450396>.
- ¹⁸A. Laaksonen and I. Napari, “Breakdown of the capillarity approximation in binary nucleation: A density functional study,” *J. Phys. Chem. B* **105**, 11678 (2001).
- ¹⁹D. W. Oxtoby and R. Evans, “Nonclassical nucleation theory for the gas–liquid transition,” *J. Chem. Phys.* **89**, 7521–7530 (1988), <https://doi.org/10.1063/1.455285>.
- ²⁰N. V. Alekseechkin, “Surface effects in droplet nucleation,” *J. Aerosol Sci.* **116**, 1–24 (2018).
- ²¹L. Gránásky, “Diffuse interface theory of nucleation,” *J. Non-Cryst. Solids* **162**, 301–303 (1993).
- ²²J. W. Cahn, “Critical point wetting,” *J. Chem. Phys.* **66**, 3667–3672 (1977).
- ²³P.-G. De Gennes, “Wetting: statics and dynamics,” *Rev. Mod. Phys.* **57**, 827 (1985).
- ²⁴D. Bonn and D. Ross, “Wetting transitions,” *Rep. Prog. Phys.* **64**, 1085–1163 (2001).
- ²⁵J. Galanis and Y. Tsori, “Mixing-demixing phase diagram for simple liquids in nonuniform electric fields,” *Phys. Rev. E Stat. Nonlin. Soft Matter Phys.* **88** 1, 012304 (2013).
- ²⁶J. Curtius, E. R. Lovejoy, and K. D. Froyd, “Atmospheric ion-induced aerosol nucleation,” in *Solar Variability and Planetary Climates* (Springer New York, New York, NY, 2006) pp. 159–167.